

## Identification of hidden orbital contributions in the $\text{La}_{0.65}\text{Sr}_{0.35}\text{MnO}_3$ valence band

F. Offi<sup>1</sup>, K. Yamauchi<sup>2</sup>, S. Picozzi<sup>3</sup>, V. Lollobrigida<sup>1</sup>, A. Verna<sup>1</sup>, C. Schlueter<sup>4</sup>, T.-L. Lee<sup>5</sup>, A. Regoutz<sup>6</sup>, D. J. Payne<sup>7</sup>, A. Petrov<sup>8</sup>, G. Vinai<sup>1</sup>, G. M. Pierantozzi<sup>8</sup>, T. Pinelli<sup>1,8,\*</sup>, G. Panaccione<sup>1,8,†</sup>, and F. Borgatti<sup>1,9</sup>

<sup>1</sup>Dipartimento di Scienze, Università Roma Tre, I-00146 Rome, Italy

<sup>2</sup>Institute of Scientific and Industrial Research, Osaka University, Ibaraki, Osaka 567-0047, Japan

<sup>3</sup>Istituto SPIN, Consiglio Nazionale delle Ricerche (CNR), sede temporanea di Chieti, c/o Università G. D'Annunzio, I-66100 Chieti, Italy

<sup>4</sup>Photon Science, Deutsches Elektronen-Synchrotron DESY, D-22607 Hamburg, Germany

<sup>5</sup>Diamond Light Source Ltd., Harwell Campus, Didcot OX11 0DE, United Kingdom

<sup>6</sup>Department of Chemistry, University College London, 20 Gordon Street, London WC1H 0AJ, United Kingdom

<sup>7</sup>Department of Materials, Imperial College London, London SW7 2AZ, United Kingdom

<sup>8</sup>Istituto Officina dei Materiali (IOM), Consiglio Nazionale delle Ricerche (CNR), Laboratorio TASC, Area Science Park, I-34149 Trieste, Italy

<sup>9</sup>Istituto per lo Studio dei Materiali Nanostrutturati (ISMN), Consiglio Nazionale delle Ricerche (CNR), I-40129 Bologna, Italy



(Received 2 February 2021; accepted 28 September 2021; published 7 October 2021)

Hybridization of electronic states and orbital symmetry in transition metal oxides are generally considered key ingredients in the description of both their electronic and magnetic properties. In the prototypical case of  $\text{La}_{0.65}\text{Sr}_{0.35}\text{MnO}_3$  (LSMO), a landmark system for spintronics applications, a description based solely on Mn 3d and O 2p electronic states is reductive. We thus analyzed elemental and orbital distributions in the LSMO valence band through a comparison between density functional theory calculations and experimental photoelectron spectra in a photon energy range from soft to hard x rays. We reveal a number of hidden contributions, arising specifically from La 5p, Mn 4s, and O 2s orbitals, considered negligible in previous analyses; our results demonstrate that all these contributions are significant for a correct description of the valence band of LSMO and of transition metal oxides in general.

DOI: 10.1103/PhysRevMaterials.5.104403

### I. INTRODUCTION

Defining the electronic structure in the valence and conduction bands of a solid is often the key problem in order to determine its electronic, structural, and, eventually, magnetic properties. This task may be particularly challenging in the case of compound materials, upon trying to clarify the role of the different elements. In general, the elemental and orbital contributions to the occupied valence states, i.e., the electronic states with binding energy at or below the Fermi energy, contain significant information on the underlying electronic structure, the hybridization among the ions, and the type of the chemical bonding [1]. Disentangling these contributions is not always an easy task, although it might be the only way to describe specific aspects of the macroscopic behavior of the materials, such as the conduction electron character in Ag, defined by the negligible presence of the correlated 4d orbital states to the conduction electrons compared to the prominent 5d contribution in gold [2]; the energy position of the valence band maxima in oxides compounds, determined by the orbital character of the cation [3]; or the metallic nature of  $\beta\text{-PbO}_2$  determined by the energy position of Pb 6s electrons [4].

The case of the perovskite  $\text{La}_{0.65}\text{Sr}_{0.35}\text{MnO}_3$  (LSMO) is particularly relevant, because of the potential applications in the field of spintronics based on its high spin polarization and colossal magnetoresistance [5]. Hybridization, symmetry, and occupation of the Mn 3d band are generally considered the key ingredients to correctly describe the electronic and magnetic properties of LSMO, along with the influence of defects such as oxygen vacancies [6]. However, the actual picture must be somewhat more complex, as witnessed, for example, by the fact that the 100% spin polarization observed at the Fermi level [7] did not find confirmation either from theoretical calculations or from measurements of spin polarization performed with different techniques [8,9], hence suggesting that a sole description of the LSMO valence states in terms of Mn d character, hybridized with O p states, is reductive. Distinguishing *all* the contributions in advance of the usual focus on Mn and O terms is therefore significant to unveil further details of the electronic structure for this complex material.

In the present work we use photoelectron spectroscopy at different photon energies, ranging from soft to hard x rays, compared with theoretical calculations in order to unravel the element and orbital contributions in the valence band of LSMO thin films, disentangling those portions that can be directly connected with the bulk electronic structure. Photoelectron spectroscopy (PES), in connection with *ab initio* calculations, was successfully exploited to recognize the LSMO valence band features, and to identify the role of

\*Present address: Department of Physical Chemistry, Fritz-Haber-Institut, 14195 Berlin, Germany.

†panaccione@iom.cnr.it

nonstoichiometric effects such as oxygen vacancies on the electronic structure [10,11]. The use of different photon energies in a large energy range takes advantage of the large dependence of the photoionization cross sections for the different orbital states on the photon energy adopted for the measurements. This approach enhances or suppresses the elemental and orbital contributions to the valence spectrum, thus providing a powerful method in order to highlight their role. In this framework, the study of the LSMO valence states by hard x-ray photoelectron spectroscopy (HAXPES), with excitation photon energies larger than 2 keV, enhances the sensitivity to specific orbital components usually not achievable for lower excitation photon energies through the more favorable contributions of the *sp/d* photoionization cross sections and specific experimental geometries [12–16]. This approach has revealed, for example, the importance of the rare-earth-*5p* contribution in the valence band spectrum of rare-earth compounds containing *3d* transition metal oxides [17], and has outlined the similarities in the O *2p* and Ir *5d* hybridization process in several double perovskites containing Ir [18]. In particular, in the present contribution we show that the joint soft x-ray photoelectron spectroscopy (SXPES)/HAXPES investigation allows to distinguish in detail the orbital distribution of the different element in the LSMO valence band spectra, hence highlighting spectral terms, especially close to the Fermi energy, which are usually hidden and thus overlooked.

## II. METHODS

The LSMO thin films have been grown by molecular beam epitaxy (MBE) at the NFFA MBE cluster setup [19] located at the APE beamline of the Elettra synchrotron radiation facility (Basovizza, Trieste, Italy). The temperature of the substrate, a SrLaAlO<sub>4</sub> (SLAO) single crystal, was set at 1000 K during growth and the O<sub>3</sub> pressure during deposition was set at  $5 \times 10^{-5}$  Pa. The 100 unit cells (around 40 nm) thick films were almost completely relaxed as concluded by x-ray diffraction (XRD) experiments (not shown).

Photoelectron spectra have been acquired at the I09 beamline [20] of the Diamond Light Source, Ltd. (Didcot, United Kingdom). The end station of the beamline is equipped with a SCIENTA EW-4000 electron energy analyzer, mounted with the lens axis perpendicular to the x-ray propagation direction. Three photon energies were used, whose nominal values are 5.94, 2.5, and 1.0 keV. An almost grazing incidence geometry (i.e., almost normal photoelectron emission direction) has been used with 3.4° angle between the x-ray direction and the sample surface, resulting in a  $30 \times 250 \mu\text{m}^2$  beam footprint on the sample surface. The specimens were measured at a temperature  $T = 200$  K, well in the metallic and ferromagnetic phase. The position of the Fermi level  $E_F$  and the overall energy resolution (beamline + analyzer) have been estimated by measuring the Fermi edge of polycrystalline Au foil in thermal and electric contact with the samples resulting in an energy resolution of  $\Delta E = 250$  meV.

Density functional theory (DFT) calculations were carried out by a projector augmented wave method implemented in the Vienna *ab initio* Simulation Package (VASP) code [21], with the generalized gradient approximation (GGA) [22]. The rotationally invariant GGA+*U* method was employed to

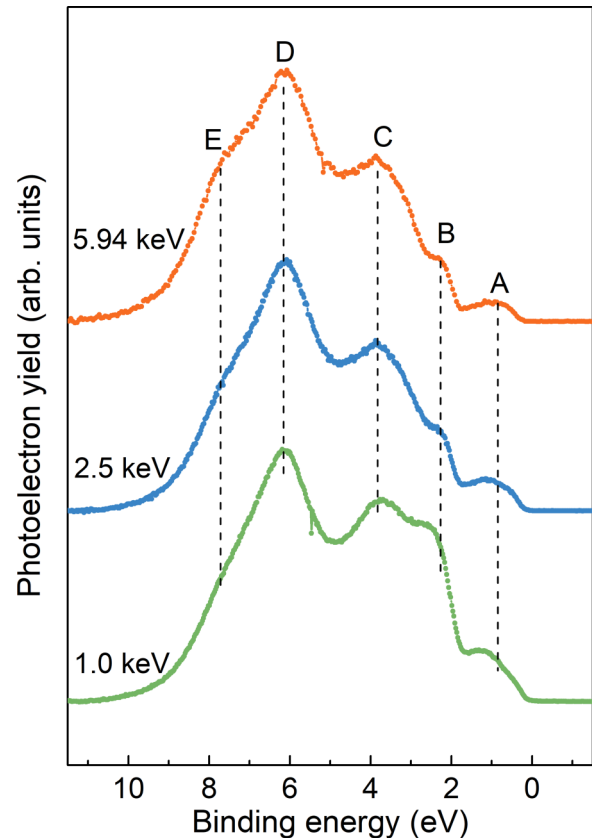


FIG. 1. Valence band SXPES and HAXPES spectra from LSMO taken at a temperature of  $T = 200$  K at different photon energies. Capital letters indicate the main structures of the spectra and are discussed in the text.

account for correlation effects [23]. The Coulomb parameter  $U$  for Mn *3d* orbital states was fixed to a small value,  $U = 1.0$  eV, allowing the best agreement with the experiment (see below). As done in previous works [24–26], a [001]-ordered (SrMnO<sub>3</sub>)<sub>1</sub>/(LaMnO<sub>3</sub>)<sub>2</sub> supercell was used, namely with a unit cell with a vertical lattice parameter that is three times the out-of-plane lattice parameter of LSMO. This setting reduces the symmetry of perovskite structure to the *P4/mmm* space group and differentiates the Mn atoms into two nonequivalent sites. Spin momenta of those three Mn atoms within a unit cell are aligned ferromagnetically. The atomic positions were relaxed until the forces were less than 0.01 eV/Å. The cutoff energy for the plane-wave expansion of the wave functions was set to 400 eV, and a  $\Gamma$ -centered  $12 \times 12 \times 4$  *k*-point mesh was used for the Brillouin zone integration for the atomic relaxation and the density of states (DOS) calculations. The Wigner-Seitz radii were set as 1.535, 2.138, 1.323, 0.820 Å for La, Sr, Mn, O, respectively. For each atomic species, we evaluated the *s*, *p*, *d* orbital-projected wave function of each band (we neglected the contribution of *f* orbitals; in particular Mn 4*f* is negligible with respect to Mn 4*s* and Mn 4*p*).

## III. RESULTS AND DISCUSSION

In Fig. 1 we show the valence band SXPES and HAXPES spectra from the LSMO film at the three different photon

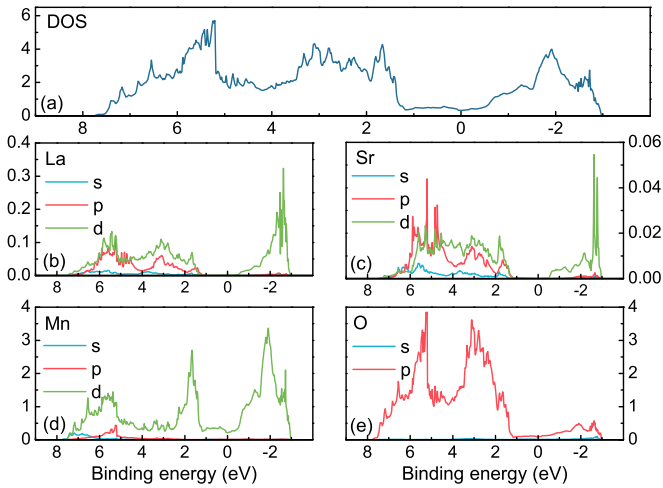


FIG. 2. Total DOS (a) and orbitally projected DOS calculated for lanthanum (b), strontium (c), manganese (d), and oxygen (e) in the LSMO compound.

energies of 5.94, 2.5, and 1.0 keV. The main structures of the spectra, labeled with capital letters (A–E), remain the same at the three photon energies, but the relative weight changes remarkably. According to the assignment of Picozzi *et al.* on the basis of previous DFT calculations [10], A and D peaks refer to the position of Mn 3d  $e_g$  and O 2p bands, respectively, while the B and C structures originate from Mn 3d  $t_{2g}$  states hybridized with oxygen. The shoulder at about 8 eV binding energy (BE), labeled as E, particularly visible in the highest photon energy spectrum, was not addressed in that work, being not visible in PES spectra with  $h\nu = 1.254$  keV primary excitation energy.

In order to fully identify all the elemental and orbital contributions occurring in the data, DFT calculations were performed for the LSMO compound by the same approach as used in Ref. [10]. Figure 2(a) shows the calculated density of states (DOS) and the *per-orbital* projected density of states (PDOS) for each element of LSMO, namely lanthanum (b), strontium (c), manganese (d), and oxygen (e). We show here the contribution of each element averaged over nonequivalent atomic sites of the lattice, and summed over the two spin directions. In the spin-resolved calculations (not shown) the system is nearly half metallic with the bare GGA approach, showing a large band gap ( $\sim 2$  eV) for the minority spin state, however, with the bottom of the conduction band slightly lower than the Fermi energy. Only upon introduction of on-site Coulomb interaction  $U$  with a small value  $U = 1$  eV, the Fermi energy enters the gap making the system half metallic. Note that the main contributions to the total DOS come from oxygen and manganese, with the intensity of lanthanum and strontium being one order and almost two orders of magnitude smaller, respectively.

Building on the DFT calculations, the experimental spectra at the different photon energies have been simulated to identify the relevance of the elemental and orbital contributions [27,28]. In this regard, it is essential to take into account the photoionization cross section for each orbital subshell. Figure 3 reports the *per-electron* cross section values for the subshells of the elements of interest from Refs. [29–31]. In

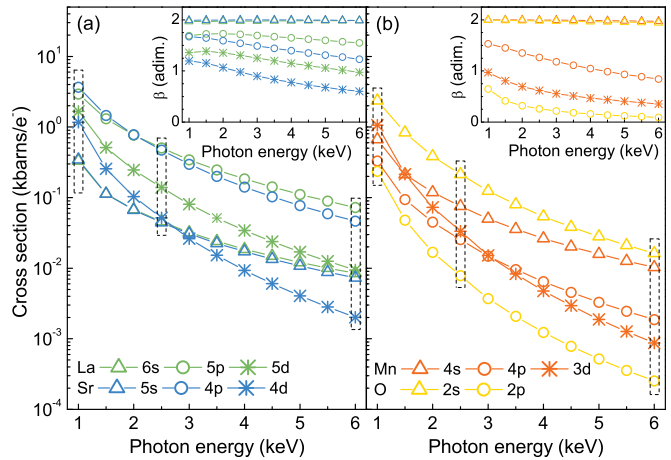


FIG. 3. Atomic *per electron* photoionization cross section values for the different valence band orbitals and the different LSMO elements, namely La and Sr (a) and Mn and O (b), versus photon energy. Different colors indicate different elements, while different symbols refer to different orbitals, namely  $s$  (triangles),  $p$  (circles), and  $d$  (asterisks). Dashed rectangles outline the cross section values for the photon energy of 1.0 keV, 2.5 keV, and 5.94 keV used for exciting the experimental spectra. In the inset of both panels the trend of the asymmetry parameter  $\beta$  versus photon energy is also shown.

particular, in Fig. 3(a) the values for La and Sr are reported, while in Fig. 3(b) the values for Mn and O are shown. Dashed rectangles outline the cross section values for the photon energy of 1.0 keV, 2.5 keV, and 5.94 keV used in the experiment. Note that the decreasing rate of the photoionization cross section, upon increasing photon energy, is not the same for all the orbitals involved. In particular, going from the soft to hard x-ray energy range favors significantly the  $s$  and  $p$  states with respect to the  $d$  states. For example, the photoionization cross section of Mn 3d is about 1.4 times larger than that of Mn 4s at 1.0 keV, but it is more than one order of magnitude smaller at 5.94 keV. A huge variation of the PDOS contributions to the valence spectra, measured over such a wide range of the excitation photon energy, is thus expected.

In particular, we recall that in the dipole approximation the differential photoionization cross section  $\sigma$  is given by the following formula [32],

$$\frac{d\sigma}{d\Omega} = \frac{\sigma}{4\pi} \left[ 1 + \beta \left( \frac{3}{2} \cos^2 \theta - \frac{1}{2} \right) \right], \quad (1)$$

where  $\beta$  is the so-called asymmetry parameter and  $\theta$  is the angle between the photon propagation direction and the electron emission direction. From this formula we calculate the total subshell photoionization cross section using tabulated values on an electron basis (see Fig. 3) through integrating over the angular acceptance of the electron analyzer of about  $0.268\pi$  sr (i.e., a cone of aperture  $\pm 30^\circ$ ).

It is worth noting that in the DFT calculations the  $s$ ,  $p$ , and  $d$  orbital contributions have been included, but it is not *a priori* obvious to which principal quantum number they refer. For example, in the Mn valence band the choice of 3d and 4s photoionization cross section for weighting the corresponding Mn  $s$  and  $d$  contributions is straightforward, but the 4p orbital,

being empty in atomic configuration, would not contribute at all as a photoionization cross section. In order to solve this problem, we followed the same approach as that suggested by Mudd *et al.*, which estimated the Cd 5p shell cross section, unoccupied in a Cd atom, by applying the In 5p/In 5s ratio to the Cd 5s cross section [33]. That is, they looked to the element next to Cd in the periodic table with at least one electron in the 5p shell (In) and to evaluate the unknown Cd 5p cross section they assumed that the cross sections ratio 5p/5s is the same for In and Cd, thus  $\sigma_{\text{Cd-}5p} = \sigma_{\text{Cd-}5s} \times \sigma_{\text{In-}5p}/\sigma_{\text{In-}5s}$ . By using the same argument, we estimated the photoionization cross section of Mn 4p (Sr 4d) by applying the Ga 4p/Ga 4s (Y 4d/Y 4p) ratio to the Mn 4s (Sr 4p) cross section, respectively. A different approach has been used in the case of lanthanum, based on the calculation of Takegami *et al.* that finds the contribution of the La 6p two orders of magnitude smaller than the one of La 5p in LaCoO<sub>3</sub>. Given the similarity of the two compounds (both are 3d transition metal oxides containing rare-earth elements) we also conclude that the La p density of states in the valence band region originates primarily from the La 5p orbital contribution included in the DFT calculation [17]. Furthermore, in analogy with the La case, we assumed that the Sr p valence states originate from the Sr 4p, although we cannot exclude that such contribution might be related to hybridization effects. Indeed, the precise assessment of the origin of the electronic charge in the less intense PDOS contributions to the valence states of manganites has been poorly addressed, since the discussion very often involves primarily the Mn 3d, O 2s, and O 2p states, while most of the other angular-momentum projected contributions are usually neglected and scarcely reported in the literature. On the other hand, as will be clear from the present work, the spectral weight of these terms can be enhanced by properly varying the photon energy, thus suggesting that all of them should be considered in the joint discussion of experimental and DFT results. Our choice is actually justified *a posteriori* by the good agreement with the experiment since, similarly to the La, the cross section for the Sr 5p orbital can be estimated about one order of magnitude smaller than for Sr 4p; however the very small contribution of Sr to the valence states—about two orders of magnitude less than Mn and O—indicates a large degree of ionic character between Sr and the host lattice, hence suggesting that the hybridization of Sr with the oxygen ions is likely small.

In order to obtain the best comparison between experimental spectra and DFT theoretical calculations, Bagheri *et al.* pointed out recently that it is necessary to consider also the fraction of charge that is located outside the atomic sphere defined for each element [34]. Each PDOS, indeed, is calculated only taking into account the electronic charge located within the atomic sphere, but, in reality, some amount of charge is distributed in the so-called interstitial region, namely the space outside the atomic spheres. This condition is particularly relevant for the s and p orbitals of Mn, being more delocalized compared with the d states, thus leading to an underestimation of the PDOS for smaller angular momenta. It may appear as a surprise to associate a specific orbital character to the interstitial, delocalized electrons. On the other hand, the success of the used approach may be a further evidence of highly localized valence hole as final state effects of the

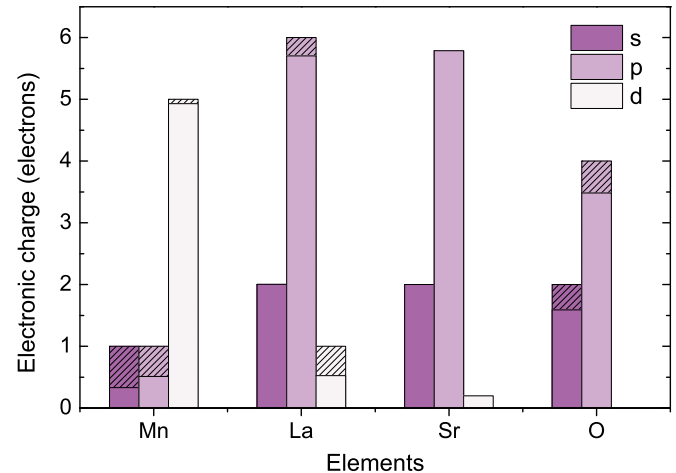


FIG. 4. Electronic charge for each element and each orbital. The shaded area correspond to the fraction of charge outside the atomic spheres.

photoemission process, as proposed by Osterwalder *et al.* for both ultraviolet [35] and x-ray excited [36] PES.

A pictorial view of the electronic charge distribution for the different elements and the different orbitals is shown in Fig. 4, where the filled rectangles represent the amount of the electronic charge integrated in the atomic spheres in the calculated configuration. The shaded areas represent, for each orbital, the amount of charge that has to be added to reach the atomic electronic configuration for each element, located in the interstitial region between the rigid atomic spheres. In some cases the orbital assignment of this charge is somewhat empirical and it was carried out following a criterion of reasonableness. For example, the electronic configuration of Mn is 3d<sup>5</sup> 4s<sup>2</sup>, and thus it is clear that one has to assume an interstitial charge of d character in order to reach the d<sup>5</sup> configuration; however, the calculations forecast also charge of p character, and thus we added interstitial charge in order to reach an s<sup>1</sup>p<sup>1</sup> electronic configuration. In any case, as shown in Fig. 4, a little amount of d charge is allowed to reach the 5 electrons of the atomic Mn configuration, while a larger amount of interstitial charge has to be assigned to both s and p orbitals to obtain 2 sp electrons. Note that with this assignment only about 30% of the Mn 4s would be located within the atomic spheres, the rest being spread over the interstitial region. We anticipate that this choice is fundamental for explaining the structure labeled E in Fig. 1. As a result, if an orbital is located for a certain amount in the interstitial region, the contribution to the total DOS of the corresponding PDOS will be underestimated by the same amount. Thus, each partial density of state has been weighted with the inverse of the fraction of charge located inside the atomic spheres, in order to estimate correctly each orbital contribution. Sr has been treated differently: since the amount of d character charge provided by the calculations is about the same as the missing charge to reach a p<sup>6</sup> electronic configuration, it was not necessary to add any interstitial charge.

Each PDOS, weighted by the appropriate photoionization cross section and corrected for the inverse electronic charge fraction inside the atomic sphere, was multiplied by the Fermi

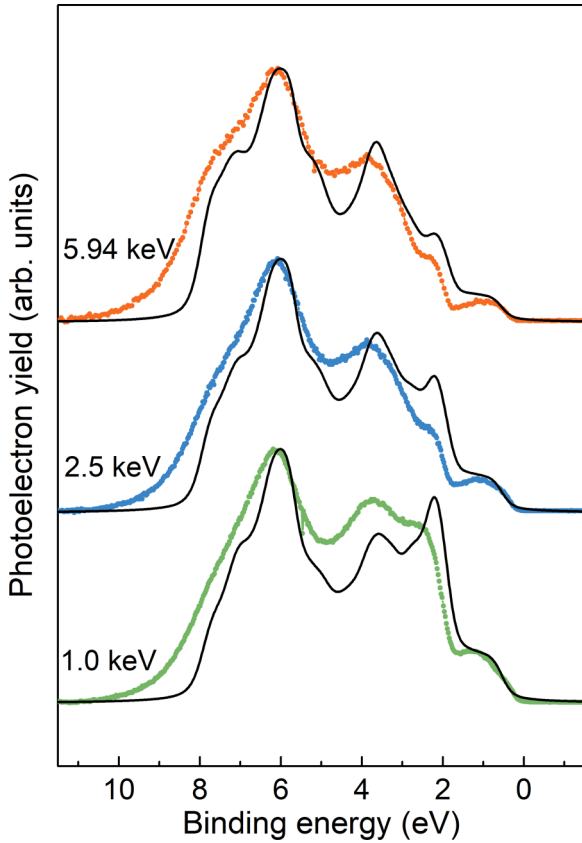


FIG. 5. Comparison of the calculated DOS (black lines) with the experimental spectra for  $h\nu = 1.0$  keV,  $h\nu = 2.5$  keV, and  $h\nu = 5.94$  keV.

distribution curve at a temperature  $T = 200$  K, as used to collect the experimental spectra. The resulting curve was then convoluted for a Gaussian function with full width at half maximum (FWHM) of 0.25 eV, fixed by the experimental resolution, and a Lorentzian function with a FWHM of 0.25 eV, chosen for the best agreement between calculations and experimental curves, and finally scaled accordingly to the LSMO stoichiometry. The resulting weighted total DOSs for the different photon energies are displayed in Fig. 5 compared with the corresponding experimental spectra. From the figure one sees that the evolution of the line shape of the experimental DOS with photon energy is consistent with the theoretical expectation based on the calculated DOS weighted by the cross section and the fraction of charge. This is particularly evident for the spectra taken at the highest photon energies of 2.5 keV and 5.94 keV. In fact, in these cases, the spectra are representative of the bulk electronic structure, and are also closer to the situation of representing a matrix-element-weighted DOS [37]. On the other hand, the experimental valence band spectrum obtained with  $h\nu = 1$  keV is quite different from the other two obtained at  $h\nu = 2.5$  keV and  $h\nu = 5.94$  keV, and also the comparison with the theoretical calculation is less satisfactory, especially the intensity of the peaks located at about 2 eV and 3.5 eV of binding energy. A possible explanation is the influence of surface-derived effects, more important at lower photon energy: contamination, different stoichiometry, defects, and real termination all can influence

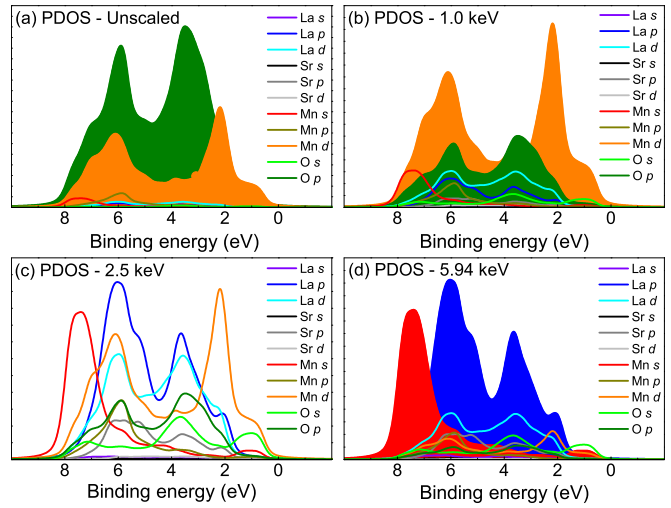


FIG. 6. Calculated PDOSs are shown unscaled (a) and weighted (b)–(d) according to the procedure described in the text.

the details of the valence band spectrum. Furthermore, the difference between surface and bulk electronic properties in LSMO is also an intrinsic effect due to reduced coordination, inducing a change of electron hybridization [38]. This has been clearly observed in core level spectra [39,40], but could also be responsible of the difference observed here in valence band spectra. The same kind of analysis was performed by comparing the experimental spectra with DFT calculations obtained with different  $U$  values, namely  $U = 2$  and  $U = 3$  (not shown). The best agreement between experiment and theory resulted indeed by the use of  $U = 1$  eV, as testified by the results of a  $\chi^2$  test and residuals analysis.

In order to realize which orbital component contributes most to each spectrum, Fig. 6 reports the PDOS, as obtained directly from the DFT calculations, that we labeled “unscaled” [Fig. 6(a)], and weighted according to an energy of  $h\nu = 1.0$  keV [Fig. 6(b)],  $h\nu = 2.5$  keV [Fig. 6(c)], and  $h\nu = 5.94$  keV [Fig. 6(d)]. The color code is the same in all panels, but the two main orbital contributions in each panel, when identifiable, are shown patterned. The unscaled DFT calculations describe a DOS that is largely dominated by the O  $p$  and the Mn  $d$  contributions, but then at the different energies the weight of the different orbitals is markedly different: while at  $h\nu = 1.0$  keV [Fig. 6(b)] the spectrum is still dominated by the Mn 3 $d$  and O 2 $p$  contributions, at the highest photon energy of  $h\nu = 5.94$  keV [Fig. 6(d)] the La 5 $p$  and the Mn 4 $s$  give origin to much of the spectrum, while at the intermediate energy of  $h\nu = 2.5$  keV [Fig. 6(c)] several components participate. Note also that the different orbitals may contribute at similar energies; thus it appears not correct to claim that at certain energies we find a contribution of a specific orbital of a material. The point of view is instead completely different: upon exciting with a selected photon energy we are able to selectively enhance or depress the contribution of some orbital components, often independent of how much they contribute to the total DOS.

In particular, the fact that at the highest primary photon energy [Fig. 6(d)] the spectrum is dominated by La 5 $p$  and Mn 4 $s$ , at the bottom of the valence band, is a consequence of

the general consideration that the favorable  $d/sp$  cross section ratio in HAXPES spectra allows us to distinguish the orbital contributions that are hidden at lower photon energies [12]. For example, the contribution of Mn 4s at the bottom of the valence band is relevant to describe the structure labeled  $E$  in Fig. 1. While the unscaled PDOS shown in Fig. 6(a) tells us that the LSMO valence band is dominated by structures attributable to Mn  $d$  and O  $p$ , upon measuring an experimental spectrum we correctly describe the different features only by properly weighting the different partial DOSs.

These considerations also reinforce the observation that the description of the electronic structure of the rare-earth compounds containing  $3d$  metals cannot avoid taking into account the contribution of the rare-earth  $5p$  shell, as put forward by Takegami *et al.* [17]. As observed, the valence band spectrum calculated for  $h\nu = 5.94$  keV [Fig. 6(d)] is dominated by the La  $5p$  orbital component. This contribution was not present in the previous assignations made by Picozzi *et al.* [10] that recognized in the valence band the O  $2p$  and Mn  $3d$  bands only, disentangling the structures originating from the  $e_g$  and  $t_{2g}$  states hybridized with oxygen.

A particular comment has to be made on the energy region close to the Fermi level, whose description thus appears more articulated than previously thought: not only the Mn  $3d$  is relevant, but also the Mn 4s and the O 2s. This is not a special feature of LSMO. For example in TiO<sub>2</sub> the chemical bonding has been connected not only to the presence of Ti  $3d$  and O  $2p$ , but also to the contribution of Ti 4s and 4p and, as is in the present case, of O 2s [41]. The approach used in the present work thus allows us the identification of orbital components that were unexpected according to previous experiments and

that can be particularly relevant for describing transport phenomena. Indeed, the fact that the more delocalized Mn 4s and the O 2s states are essential for describing the region close to the Fermi level nicely explains the fact that the near Fermi level spectral weight can be used as a measure of the variation of electrical conductivity better in the HAXPES than in the SXPE regime [42].

#### IV. CONCLUSIONS

We have analyzed photoelectron spectra from LSMO films obtained in a large photon energy range, such that the contribution of the different elemental and orbital components is largely modulated by the variation of the photoionization cross section. A detailed comparison with DFT calculations allows us to identify the contribution of orbital components that had previously been overlooked. While the hybridized Mn  $3d$  and O  $2p$  states give rise to most of the DOS, the contribution of states such as La  $5p$ , Mn 4s, and O 2s is not irrelevant and becomes fundamental to properly describe the spectral shape, especially in the HAXPES regime. We thus put forward the idea that such states have to be taken into account to properly describe the physical and chemical properties of LSMO.

#### ACKNOWLEDGMENTS

We gratefully thank L. H. Tjeng for fruitful suggestions. This work has been partially performed in the framework of the Nanoscience Foundry and Fine Analysis (NFFA-MUR Italy Progetti Internazionali) project [43].

- 
- [1] A. Walsh, A. A. Sokol, J. Buckeridge, D. O. Scanlon, and C. R. A. Catlow, *Nat. Mater.* **17**, 958 (2018).
  - [2] A. Sekiyama, J. Yamaguchi, A. Higashiya, M. Obara, H. Sugiyama, M. Y. Kimura, S. Suga, S. Imada, I. A. Nekrasov, M. Yabashi, K. Tamasaku, and T. Ishikawa, *New J. Phys.* **12**, 043045 (2010).
  - [3] S. Li, J. Morasch, A. Klein, C. Chirila, L. Pintilie, L. Jia, K. Ellmer, M. Naderer, K. Reichmann, M. Grötting, and K. Albe, *Phys. Rev. B* **88**, 045428 (2013).
  - [4] D. J. Payne, R. G. Edgell, G. Paolicelli, F. Offi, G. Panaccione, P. Lacovig, G. Monaco, G. Vanco, A. Walsh, G. W. Watson, J. Guo, G. Beamson, P.-A. Glans, T. Learmonth, and K. E. Smith, *Phys. Rev. B* **75**, 153102 (2007).
  - [5] A. Bhattacharya and S. J. May, *Annu. Rev. Mater. Res.* **44**, 65 (2014).
  - [6] S. Kumari, N. Mottaghi, C.-Y. Huang, R. Trappen, G. Bhandari, S. Yousefi, G. Cabrera, M. S. Seehra, and M. B. Holcomb, *Sci. Rep.* **10**, 3659 (2020).
  - [7] J.-H. Park, E. Vescovo, H.-J. Kim, C. Kwon, R. Ramesch, and T. Venkatesan, *Nature (London)* **392**, 794 (1998).
  - [8] B. Nadgorny, *J. Phys.: Condens. Matter* **19**, 315209 (2007).
  - [9] B. Nadgorny, I. I. Mazin, M. Osofsky, J. R. J. Soulen, P. Broussard, R. M. Stroud, D. J. Singh, V. G. Harris, A. Arsenov, and Y. Mukovskii, *Phys. Rev. B* **63**, 184433 (2001).
  - [10] S. Picozzi, C. Ma, Z. Yang, R. Bertacco, M. Cantoni, A. Cattoni, D. Petti, S. Brivio, and F. Cicacci, *Phys. Rev. B* **75**, 094418 (2007).
  - [11] H. Guo, J. Wang, X. He, Z. Yang, Q. Zhang, K. Jin, C. Ge, R. Zhao, L. Gu, Y. Feng, W. Zhou, X. Li, Q. Wan, M. He, C. Hong, Z. Guo, C. Wang, H. Lu, K. Ibrahim, S. Meng *et al.*, *Adv. Mater. Interfaces* **3**, 1500753 (2016).
  - [12] G. Panaccione, G. Cautero, M. Cautero, A. Fondacaro, M. Grioni, P. Lacovig, G. Monaco, F. Offi, G. Paolicelli, M. Sacchi, N. Stojic, G. Stefani, R. Tommasini, and P. Torelli, *J. Phys.: Condens. Matter* **17**, 2671 (2005).
  - [13] A. Sekiyama, A. Higashiya, and S. Imada, *J. Electron Spectrosc.* **190**, 201 (2013).
  - [14] S. Ueda and I. Hamada, *J. Phys. Soc. Jpn.* **86**, 124706 (2017).
  - [15] S. Ouardi, G. H. Fecher, X. Kozina, G. Stryganyuk, B. Balke, C. Felser, E. Ikenaga, T. Sugiyama, N. Kawamura, M. Suzuki, and K. Kobayashi, *Phys. Rev. Lett.* **107**, 036402 (2011).
  - [16] J. Weinen, T. C. Koethe, C. F. Chang, S. Agrestini, D. Kasinathan, Y. F. Liao, H. Fujiwara, C. Schüller-Langeheine, F. Strigari, T. Haupricht, G. Panaccione, F. Offi, G. Monaco, S. Huotari, K.-D. Tsuei, and L. H. Tjeng, *J. Electron Spectrosc.* **198**, 6 (2015).
  - [17] D. Takegami, L. Nicolaë, T. C. Koethe, D. Kasinathan, C. Y. Kuo, Y. F. Liao, K.-D. Tsuei, G. Panaccione, F. Offi, G. Monaco,

- N. B. Brookes, J. Minár, and L. H. Tjeng, *Phys. Rev. B* **99**, 165101 (2019).
- [18] D. Takegami, D. Kasinathan, K. K. Wolff, S. G. Altendorf, C. F. Chang, K. Hoefer, A. Melendez-Sans, Y. Utsumi, F. Meneghin, T. D. Ha, C. H. Yen, K. Chen, C. Y. Kuo, Y. F. Liao, K. D. Tsuei, R. Morrow, S. Wurmehl, B. Büchner, B. E. Prasad, M. Jansen *et al.*, *Phys. Rev. B* **102**, 045119 (2020).
- [19] G. Vinai, F. Motti, A. Y. Petrov, V. Polewczyk, V. Bonanni, R. Edla, B. Gobaut, J. Fujii, F. Suran, D. Benedetti, F. Salvador, A. Fondacaro, G. Rossi, G. Panaccione, and B. A. D. P. Torelli, *Rev. Sci. Instrum.* **91**, 085109 (2020).
- [20] T.-L. Lee and D. A. Duncan, *Synchrotron Radiat. News* **31**, 16 (2018).
- [21] G. Kresse and J. Furthmüller, *Phys. Rev. B* **54**, 11169 (1996).
- [22] J. P. Perdew, K. Burke, and M. Ernzerhof, *Phys. Rev. Lett.* **77**, 3865 (1996).
- [23] S. L. Dudarev, G. A. Botton, S. Y. Savrasov, C. J. Humphreys, and A. P. Sutton, *Phys. Rev. B* **57**, 1505 (1998).
- [24] D. J. Singh and W. E. Pickett, *Phys. Rev. B* **57**, 88 (1998).
- [25] D. J. Singh and W. E. Pickett, *J. Appl. Phys.* **83**, 7354 (1998).
- [26] C. Ma, Z. Yang, and S. Picozzi, *J. Phys.: Condens. Matter* **18**, 7717 (2006).
- [27] U. Gelius, C. J. Allan, G. Johansson, H. Siegbahn, D. A. Allison, and K. Siegbahn, *Phys. Scr.* **3**, 237 (1971).
- [28] J.-T. J. Huang and F. O. Ellison, *J. Electron Spectrosc. Relat. Phenom.* **4**, 233 (1974).
- [29] M. B. Trzhaskovskaya, V. I. Nefedov, and V. G. Yarzhemsky, *At. Data Nucl. Data Tables* **77**, 97 (2001).
- [30] M. B. Trzhaskovskaya, V. I. Nefedov, and V. G. Yarzhemsky, *At. Data Nucl. Data Tables* **82**, 257 (2002).
- [31] M. B. Trzhaskovskaya and V. G. Yarzhemsky, *At. Data Nucl. Data Tables* **119**, 99 (2018).
- [32] C. S. Fadley, in *Electron Spectroscopy: Theory, Techniques, and Applications*, edited by C. R. Brundle and A. D. Baker (Academic Press, London, 1978).
- [33] J. J. Mudd, T.-L. Lee, V. M. Muñoz-Sanjosé, J. Z. Zúñiga-Pérez, D. J. Payne, R. G. Egisdell, and C. F. McConville, *Phys. Rev. B* **89**, 165305 (2014).
- [34] M. Bagheri and P. Blaha, *J. Electron Spectrosc.* **230**, 1 (2019).
- [35] J. Osterwalder, T. Greber, P. Aebi, R. Fasel, and L. Schlapbach, *Phys. Rev. B* **53**, 10209 (1996).
- [36] J. Osterwalder, T. Greber, S. Hüfner, and L. Schlapbach, *Phys. Rev. Lett.* **64**, 2683 (1990).
- [37] C. S. Fadley, *Nucl. Instrum. Methods A* **547**, 24 (2005).
- [38] T. Pincelli, V. Lollobrigida, F. Borgatti, A. Regoutz, B. C. Schlueter, T. L. Lee, D. J. Payne, M. Oura, K. Tamasaku, A. Y. Petrov, P. Graziosi, F. M. Granozio, F. Miletto, M. Cavallini, G. Vinai, R. Ciprian, C. H. Back, G. Rossi, M. Taguchi, H. Daimon *et al.*, *Nat. Commun.* **8**, 16051 (2017).
- [39] F. Offi, P. Torelli, M. Sacchi, P. Lacovig, A. Fondacaro, G. Paolicelli, S. Huotari, G. Monaco, C. S. Fadley, J. F. Mitchell, G. Stefani, and G. Panaccione, *Phys. Rev. B* **75**, 014422 (2007).
- [40] F. Offi, N. Mannella, T. Pardini, G. Panaccione, A. Fondacaro, P. Torelli, M. W. West, J. F. Mitchell, and C. S. Fadley, *Phys. Rev. B* **77**, 174422 (2008).
- [41] J. C. Woicik, E. J. Nelson, L. Kronik, M. Jain, J. R. Chelikowsky, D. Heskett, L. E. Berman, and G. S. Herman, *Phys. Rev. Lett.* **89**, 077401 (2002).
- [42] T. Hishida, K. Ohbayashi, M. Kobata, E. Ikenaga, T. Sugiyama, K. Kobayashi, M. Okawa, and T. Saitoh, *J. Appl. Phys.* **113**, 233702 (2013).
- [43] See <http://www.trieste.NFFA.eu>.